J Musculoskelet Neuronal Interact 2014; 14(2):173-188

Original Article

Hylonome

Cholinergic nerve fibers in bone defects of a rat osteoporosis model and their regulation by implantation of bone substitution materials

K.S. Lips[1], V. Kauschke[1], S. Hartmann[1], U. Thormann[2], S. Ray[1], M. Schumacher[3], M. Gelinsky[3], S. Heinemann[4], T. Hanke[4], A.R. Kautz[5], M. Schnabelrauch[5], G. Szalay[2], C. Heiss[1,2], R. Schnettler[1,2], V. Alt[2], O. Kilian[1,6]

[1]Laboratory for Experimental Trauma Surgery, Justus-Liebig University Gießen, Kerkraderstr. 9, 35394 Gießen, Germany; [2]Department of Trauma Surgery Gießen, University Hospital of Gießen-Marburg, Justus-Liebig University Giessen, Rudolf-Buchheim-Str. 7, 35392 Gießen, Germany; [3]Center for Translational Bone, Joint, and Soft Tissue Research, Medical Faculty and University Hospital, Technische Universität Dresden, Fetscherstr. 74, 01307 Dresden, Germany; [4]Max-Bergmann-Center of Biomaterials and Institute of Material Science, Technische Universität Dresden, Budapester Str. 27, 01069 Dresden, Germany; [5]INNOVENT e.V., Biomaterials Department, Prüssingstr. 27B, 07745 Jena, Germany; [6]Department of Orthopedics and Trauma, Zentralklinik Bad Berka, Robert-Koch-Allee 9, 99437 Bad Berka, Germany

Abstract

Objectives: Bone is innervated by autonomic nervous system that consists of sympathetic and parasympathetic nerves that were recently identified in bone. Thus we asked whether parasympathetic nerves occur in bone defects and at the interface of substitution materials that were implanted for stabilization and improvement of healing in an osteoporosis animal model. **Methods:** Osteoporosis was induced in rats by ovariectomy and deficiency diet. A wedge-shaped osteotomy was performed in the metaphyseal area of femur. Eight different implants were inserted that were based on calcium phosphate cement, iron, silica-mineralized collagen, and modifications with strontium. Nerves were identified by immunohistochemistry with antibodies against vesicular acetylcholine transporter (VAChT), tyrosine hydroxylase (TH) and protein gene product 9.5 (PGP 9.5) as neuronal marker. **Results:** Cholinergic nerves identified with VAChT immunostaining were detected in defects filled with granulation tissue and in surrounding mast cells. No immunolabeling of cholinergic nerves was found after implantation. The general presence of nerves was reduced after implantation as shown by PGP 9.5. Sympathetic nerves identified by TH immunolabeling were increased in strontium functionalized materials. **Conclusion:** Since cholinergic innervation was diminished after implantation a further increase in the compatibility of substitution materials to nerves could improve defect healing especially in osteoporotic bone.

Keywords: Osteoporosis, Bone Substitution Material, Osteotomy, Vesicular Acetylcholine Transporter, Tyrosine Hydroxylase

Introduction

The systemic bone disease osteoporosis is characterized by a loss of bone mass and bone mineral content and by an increase in fracture and bone defect incidence[1]. Bone mass is regulated locally by the balance of two important processes: formation of new bone and degradation of old and damaged bone. Together they are designated as bone remodeling. Both processes are directly regulated by each other through the so called "cross talk" of the bone forming osteoblasts and bone resorbing osteoclasts with cytokines, growth factors and the system of RANK (receptor activator of nuclear factor kappa-light-chain-enhancer of activated B cells), its ligand RANKL and osteoprotegerin[2]. In addition to this direct regulation bone remodeling is controlled by the nervous system. The presence of nerve fibers in bone is well documented[3-5]. Recent investigations on knockout- (KO) mice kindled the discussion about the involvement of cholinergic nerve fibers in bone regulation[6-8]. Eimar et al. (2013) described the existence of three dif-

The authors have no conflict of interest.

Corresponding author: Katrin S. Lips, Laboratory for Experimental Trauma Surgery, Justus-Liebig University Gießen, Kerkrader Str. 9, D-35394 Gießen, Germany
E-mail: Katrin.S.Lips@chiru.med.uni-giessen.de

Edited by: F. Rauch
Accepted 28 March 2014

ferent signaling pathways for bone remodeling with attendance to the nervous system: 1) the hypothalamic-pituitary-thyroid axis, 2) the co-regulation of bone, adipose tissue and energy metabolism altered by the sympathetic system, and 3) the interleukin (IL)1-parasympathetic system-bone axis[9]. The innervation of bone by the sympathetic system is well known[10] whereas only limited reports are available that demonstrate the presence of autonomic cholinergic nerve fibers in the skeletal system directly[6,11-13] and indirectly via disruption of the vagus nerve[14]. Clinical and experimental studies on neuronal disorders and lesions showed that a reduction in innervation leads to an impaired bone growth, turnover and repair[15-19] often associated with the formation of enlarged fracture calluses, incomplete maturation of woven bone and delayed calcium accumulation[20-22]. A reduction in calcium content is also found in osteoporosis. In an osteoporotic animal model a dramatic down-regulation in the innervation density was depicted[23]. It has been hypothesized that a decrease in nerve fibers is followed by an increase in fracture incidence[21]. The stabilization of osteoporotic fracture poses still a challenge in trauma surgery. Treatment of osteoporotic bone defects requires often the insertion of bone substitution materials to improve bone healing and stabilization[24,25]. The choice of the most suitable material for osteoporotic bone is controversially discussed. Up to our knowledge it is not known whether the innervation is affected by bone substitution materials. Thus we conducted an osteoporotic animal model with osteotomy and implantation where we analyzed the presence of nerve fibers by means of immunohistochemistry. Female Spargue-Dawley rats at the age of 14 weeks were ovariectomized and fed with a calcium and vitamin C/D2/D3 deficient diet[26,27]. After 12 weeks wedge-shaped osteotomy was performed in the metaphyseal area of the distal femur. Wedge-shaped bone defects were created to mimic the clinical situation of patients with osteoporosis. Osteoporotic fractures are mainly characterized by a sintering of spongy bone that is most likely represented in a model by a wedge-shape form. Bone substitution materials were implanted into the bone defect[28-30]. Finally eight different materials were tested. All of them fulfilled the criteria of suitable bone substitution materials as they were localy and systemically biocompatible, filled the defect completely and facilitated the replacement by bone. Since none of the commercial available material is etiology tested for osteoporotic bone we decided to use several materials which most closely fulfill the requirements for an ideal bone substitution material for systemically diseased bone. One of the selected materials was bone calcium phosphate cement (CPC) with and without modification with strontium[31,32]. CPC is well-established as synthetic alternative of the gold standard bone substitute spongiosa autograft[33]. CPC has the advantage that it is freely-moldable and therefore easily introduced into bone defects. Its short setting times (between 4-15 min) qualifies CPC for clinical application[34]. It is biodegradable and can therefore be used as a drug delivery system e.g. for application of strontium[32]. Strontium increases bone formation, reduces bone degradation by osteoclasts and is frequently administered during osteoporosis treatment[29,31,35]. Besides CPC we implanted a monolithic composite xerogel comprising silica and bovine collagen type I (B30)[36]. This material is designated for bone substitution because of its unique mechanical properties[37]. Usually, collagen fibrils mineralized by calcium phosphate phases are well-approved as bone substitutes since they mimic the natural bone. In this study, the calcium phosphate mineralization is replaced by a sol-gel silicification in order to get a material possessing mechanical properties that are independent on calcium phosphate phases. The latter might be added as a powder to the reaction solution by simple mixing[36,37]. Then, their main function is binding or delivering Ca^{2+}-ions. So, this material with or without calcium phosphate phases is able to manipulate the osteoblast/ osteoclast ratio in a corresponding human co-culture model[38]. In this study we focus on the calcium phosphate free basic material B30 that has been already successfully implanted in a tibia fracture in rats[30]. In general, silica is considered to improve the osteogenic potential of biomaterials for bone regeneration[39].

In addition to the monolithic B30 xerogel the same composite was implanted as particles entrapped in a porous collagen scaffold (pB30) in order to increase the degradation time. Here, the B30 xerogel particles were further modified with strontium carbonate (pB30S20) since features of strontium are adjuvant for osteoporotic bone[35].

Moreover we inserted metallic implants build up by iron. First usage of iron was investigated for cardiovascular stents that exhibited *in vivo* neither distinct inflammatory reaction nor altered serum levels or cytotoxic effects[40-43]. Additional advantages of iron for usage as bone substitution material are its high mechanical strength and relatively low corrosion rate[44,45]. The iron implants were charged by interconnected pores to improve its osseous integration. In one animal group pure iron implants were inserted whereas in two additional animal groups the implants were additionally coated with either strontium or the bisphosphonate zolendronic acid. Bisphosphonates are applied as therapeutic agent after surgery of osteoporotic patients to improve implant durability[46]. Bone samples were harvested 6 weeks after osteotomy and analyzed after immunohistochemical incubations with antibodies against the pan-neuronal marker protein gene product 9.5 (PGP 9.5), tyrosine hydroxylase (TH) for sympathetic processes, and vesicular acetylcholine transporter (VAChT) for cholinergic fibers. Nerve fibers positively stained with all three antibodies were found in the granulation tissue bridging the bone defect whereas at the interface of the implants no VAChT immunopositive fibers were detected. Thus we suppose that implantation of bone substitution materials influences the presence of nerve fibers.

Materials and methods

Bone substitution materials

Randomized distributed eight different bone substitution materials were implanted in 4 mm wedge-shaped defects generated by osteotomy of the left femur. Since no suitable etiology-adapted materials are available we decided to focus on

eight different materials that most closely fulfill the demands for an ideal bone substitution material.

Calcium phosphate bone cement

Plain calcium phosphate bone cement (CPC), formulated to form nanocrystalline, carbonated hydroxyapaptite upon setting, has already been described in detail[47]. In brief, CPC precursor powder was composed of 24 wt% dicalcium phosphate ($CaHPO_4$), 8.5 wt% precipitated hydroxyapatite [$Ca_{10}(PO_4)_6(OH)_2$], 8.5 wt% calcium carbonate ($CaCO_3$) and 58 wt% of α-tricalcium phosphate [$Ca_3(PO_4)_2$]. Directly prior to implantation, a paste was prepared by manual mixing of the cement powder with an aqueous solution of 4 % Na_2HPO_4 with a liquid-to-powder ratio of 0.4 ml/g[29].

Strontium (II) modified calcium phosphate bone cement

As second material the CPC was modified with strontium as described recently[31,32]. In brief, strontium (II) modified CPC (CPC-Sr) was generated by replacement of $CaCO_3$ with strontium carbonate ($SrCO_3$) in the cement precursor powder (Sr/Ca= 0.123) (CPC-Sr). Implantation was conducted with a paste formulation of the cement powder with an aqueous solution of 4 % Na_2HPO_4 that was mixed manually. The final liquid-to-powder-ratio consisted of 0.35 ml/g[29].

Silica collagen composite xerogel

A degradable composite xerogel (B30) was used as additional biomaterial. It was composed of 70 wt% silica and 30 wt% collagen. Orthosilicic acid was produced by hydrolysis of tetra-ethoxysilane (99 % pure, Sigma, Taufkirchen, Germany) with deionized water and 0.01 M hydrochloric acid as a catalyst. Afterwards a homogeneous suspension was generated from the orthosilicic acid and 30 mg/ml fibrillar bovine collagen by mixing. After 3 days of stabilization the hydrogels were dried at 37°C and 95 % humidity in a climate chamber[36] and implanted as one solid part.

Porous collagen scaffold with composite xerogel particles

Xerogel particles of B30 with a size of <250 µm (pB30) were embedded in a collagen matrix with a xerogel/matrix weight ratio of 1.0. The porous material was inserted into the defect[28].

Strontium modified porous collagen scaffold with composite xerogel

As additional biomaterial for bone substitution the scaffolds were prepared by xerogel particles consisting of 50 wt% of silica, 30 wt% of fibrillar bovine collagen, and 20 wt% strontium carbonate (pB30S20).

Iron foam

Furthermore, iron foam with interconnected pores (Fe) was applied that was created of carbonyl iron Fe3-powder and a polyvinyl alcohol binder by sintering at 1150°C and shaping by wire eroding.

Strontium coated iron foam

As additional material group plain iron foam was coated with $SrCO_3$ H_3PO_4 (Fe-Sr) for 4 hours (h) under vacuum and was carefully rinsed with ethanol afterwards.

Bisphosphonate coated iron foam

Besides plain iron foam implants were coated with a bisphosphonate zoledronate complex salt (Fe-BP). This salt which is only sparingly soluble in water was prepared by mixing aqueous solutions of sodium zoledronate, sodium stearate, and iron(III)-chloride containing a molar ratio of zoledronate: stearate: iron(III)= 1 : 1 : 1. The precipitated salt was collected, thoroughly, washed with water, and dried under vacuum. For implant coating the zoledronate salt was finely grinded and resuspended in acetone to form a homogeneous suspension containing 35 µg of zoledronate salt (17 µg pure zoledronate). Implants were fixed in a holding device of a stirring motor and coated under stirring dropwise with the coating suspension. Afterwards, the implants were dried to completely remove acetone. All manipulations were performed under sterile conditions in a clean bench.

Animal models

Animal care and surgery were performed in accordance to the legal requirement for animal protection and approved by the government of the county (presidal government Gießen, permit Number V 54 -19 c 20-15 (1) GI 20/28 Nr. 92/2009 and V 54-19 c 20-15 (1) GI20/28 Nr. 108/2011). All the surgical procedures were performed under general anesthesia with i.p. injection of ketamine (62.5 mg/kg body weight, Hostaket, Hoechst, Germany) and xylazine (7.5 mg/kg body weight, Rompun, Bayer, Germany). Female 14-week old Sprague-Dawley rats (n=74, Charles River, Sulzfeld, Germany) underwent laparotomy followed by bilateral removal of both ovaries under strict sterile conditions. The animals were kept in the local animal facility under a 12 hour (h) light-dark cycle with free access to water and specific chow with a reduced content on calcium, vitamin C/D2/D3, and phosphate (Altromin C1034, Lage, Germany)[26,27]. After 12 weeks the animals were divided into groups to perform three different animal models.

In the first model the influence of the defect size on the innervation was tested without insertion of any bone substitution materials. Therefore, a wedge-shaped osteotomy was performed on the distal metaphyseal area of the left femur. A 3 cm skin incision was made on the distal part of the lateral thigh. After incision of the septum between lateral vastus and femoral biceps muscle the femur was exposed and subsequently fixed with a 7-hole T-shaped mini-plate to increase the stability of the bone (Stryker, Schönkirchen, Germany). Afterwards, the defects were created with an ultrasound bone saw (Piezosurgery, Mectron, Cologne, Germany). On the medial femur side the defect was 0.35 mm. In groups of 6 animals each, different defect sizes of 3, 4 and 5 mm were tested on the lateral side. Thus the distal metaphysis of the left femur was completely divided into two parts but stabilized by the 7-

hole T-shaped mini-plate. Since the 4 mm defect was identified as critical size defect this dimension was used for the osteoporosis implantation model[29].

In the second animal model several bone substitution materials were inserted in the bony defects of osteoporotic rats to investigate the effects of different materials on the presence of nerve fibers. The animals with the 4 mm empty defect from the first animal model served as controls. All other defects were filled with one of the above described materials[29]. The eight animal groups consisted of 6 animals each.

In the third animal model osteoporotic and non-osteoporotic rats were compared in 2 groups with 4 animals each. For this model only one bone substitution material was used: the composite xerogel composed of 70 wt% silica and 30 wt% collagen (B30). Before implantation the xerogel was shaped according to the defect. This was possible because of the ductile behavior of the composite material[30].

Afterwards the fascia was sutured with 3/0 vicryl and the skin closed with 4/0 prolene and additional metal clamps. After a follow-up time of 6 weeks the animals were euthanized with CO_2 inhalation after general anesthesia and the left femora was harvested[28-30].

Immunohistochemistry

Left femurs were immersion-fixed in 4 % phosphate-buffered paraformaldehyde (Merck, Darmstadt, Germany), washed in 0.1 M phosphate buffer, and embedded in methylmethacrylate (Technovit 9100, Heraeus Kulzer, Hanau, Germany). Five µm thick sections were cut with a rotation microtome (Leica RM2144, Wetzlar, Germany) using the aid of Kawamotos's film (Secton-Lab Co. Ltd., Japan) to keep the biomaterials intact. Sections were deplasticized with 3-methoxyethylacetat (MEA, Merck, Darmstadt, Germany) for 3x 20 min and rehydrated through a series of acetone and Tris-NaCl buffer with 0.025 % Trition-X-100 (wash buffer, pH 7.4). Endogenous peroxidase was blocked with 3 % H_2O_2 in wash buffer for 5 min. Sections were processed overnight (4°C) with one of the following primary antibodies diluted in dilution buffer (Dako, Glostrup, Denmark): a) polyclonal anti-rabbit PGP 9.5 diluted 1:40,000 (Biotrend, Cologne, Germany), b) polyclonal anti-goat VAChT diluted 1:28,000 (Phoenix Pharmaceuticals, Burlingame, CA, USA), and c) polyclonal anti-rabbit TH diluted 1:500 (Biotrend, Cologne, Germany). After careful washing the sections were incubated with goat anti-rabbit secondary antibody (1:500; Vector, Burlingame, CA, USA) or rabbit anti-goat secondary antibody (1:800, Dako, Glostrup, Denmark) for 30 min. Subsequently, sections were treated with ABC complex/horseradish peroxidase labeled avidin (Dako, Glostrup, Denmark) for 30 min and peroxidase activity was visualized with Nova Red (Vector, Burlingame, CA, USA). The nuclei were counterstained with hematoxylin. The stainings were analyzed both qualitatively and semi-quantitatively with a light microscope with photo-module (Axiophot 2, Zeiss, Jena, Germany) and a digital camera (Leica DC 500, Bensheim, Germany). Immunopositive structures were quantified in the granulation tissue that filled the empty defects and surrounded the implants. Quantification was performed according to a scoring scale that ranged from 0 to 4 (0=absent, 1=few, 2=moderate and 3=high amount). The evaluation was conducted with the 100x objective and in a blinded way. The score was given as mean with SD.

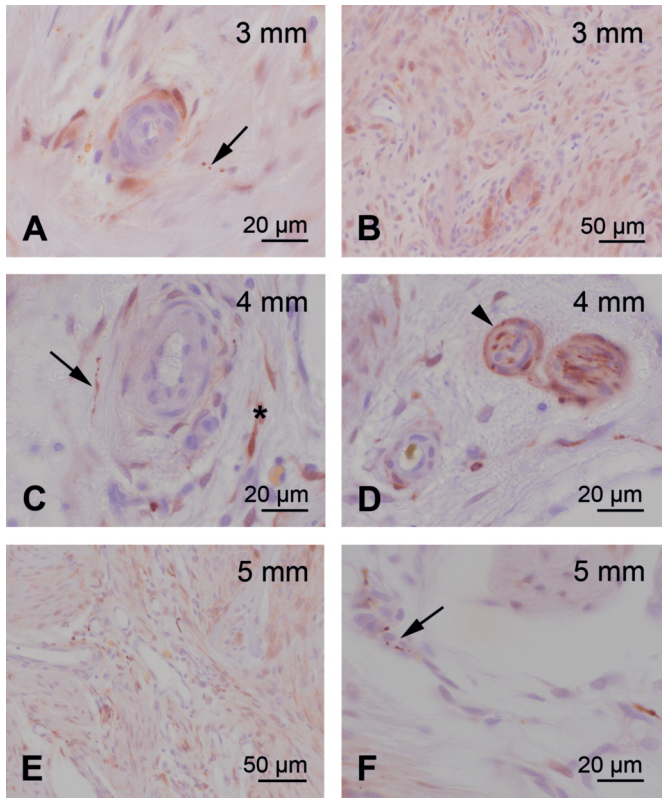

Figure 1. PGP 9.5, defect healing. PGP 9.5 labeling was found in 3 (A, B), 4 (C, D) and 5 mm sized bone defects (E, F). Nerve fibers (arrow in A, C, F), cells in the granulation tissue (B, E and star in C) and in the 4 mm defects also nerve fiber bundles (arrowhead in D) were PGP positively stained.

Statistical analysis

The non-parametric Kruskal-Wallis and Mann-Whitney tests were used for statistical analysis with the SPSS software (version 21.0, SPSS Institute Inc, Cicago, USA). A difference of $p \leq 0.05$ was defined as significant.

Results

Nerve fibers in the osteoporotic bone defect model without implantation of biomaterial`

For detection of nerve fibers pan-neuronal marker PGP 9.5 was used. PGP 9.5 labeling was found in the granulation tissue filling the osteotomy gap of all three defect sizes: 3, 4, and 5 mm (Figure 1). In the nearly bridged 3 mm defect PGP 9.5 staining was detected in nerve fibers (Figure 1A) and a high number of cells localized in the granulation tissue (Figure 1B). In the 4 mm defect a high amount of blood vessels were found

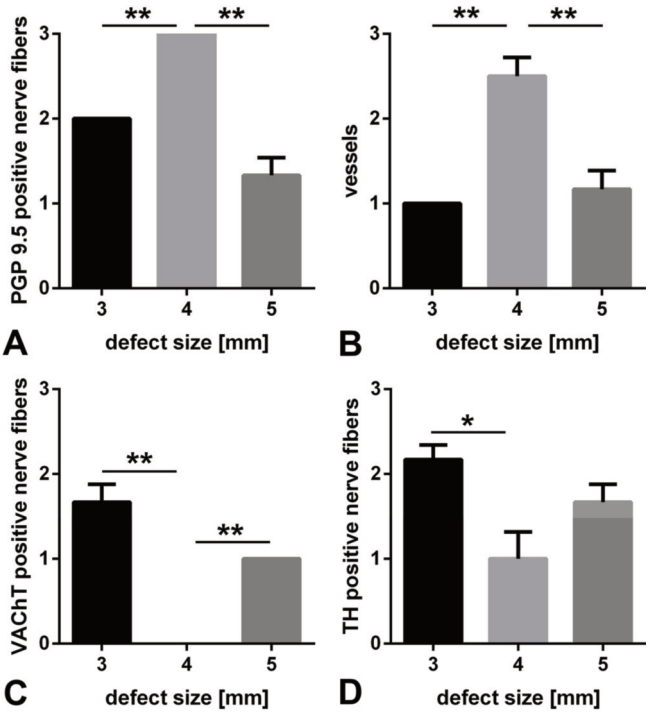

Figure 2. Empty defects with a size of 3, 4, and 5 mm revealed an increase of PGP 9.5 positive nerve fibers at the 4 mm defects (A), whereas the amount of VAChT and TH immunopositive nerve fibers were increased at the 3 mm defects. The amount of new formed vessels was also scored and resulted in a significant increase at the 4 mm defects. *p<0.05, **p<0.01; score 0=absent, 1=few, 2=moderate, and 3=high amount.

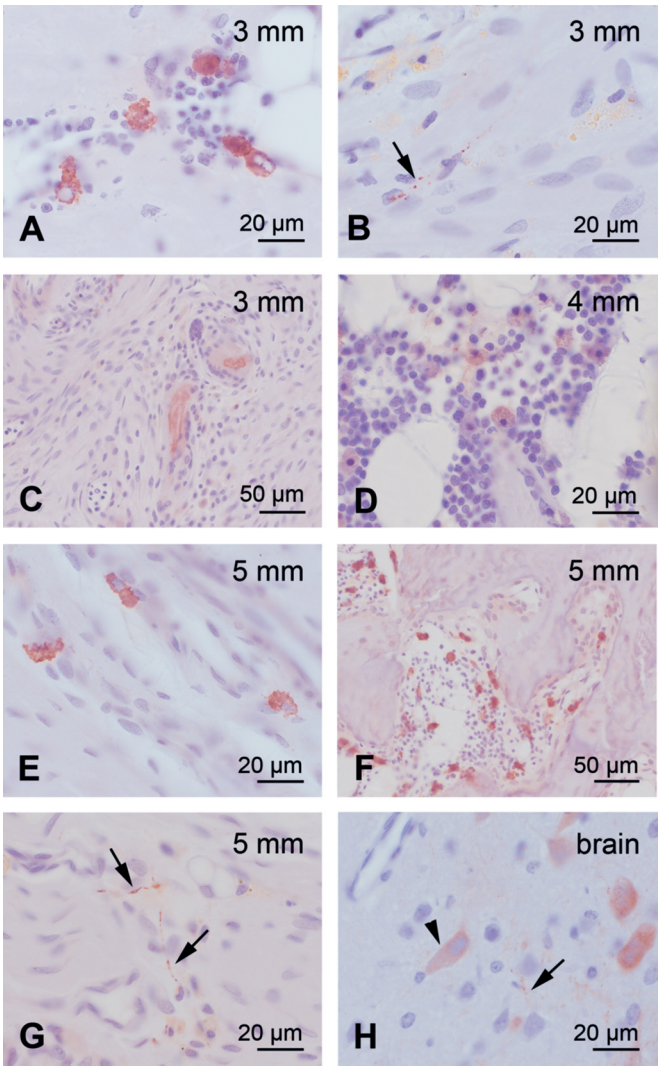

Figure 3. VAChT, defect healing. VAChT staining was found in mast cells (A, D-F), nerve fibers (arrow in B, G), and nerve fibers bundles (C) in the granulation tissue filling the defect. The immunolabeling was found in 3 and 5 mm defects whereas in the 4 mm defect only immunopositive mast cells were determined. Brain was used as positive control where neurons (arrowhead) and nerve fibers (arrow) were labeled (H).

that contained PGP 9.5 positive nerve fibers (Figure 1C) and even nerve fiber bundles were detected (Figure 1D). In the granulation tissue also some cells were labeled with PGP 9.5 (Figure 1C). The fracture gap of the 5 mm defect was extended but filled with a kind of granulation tissue (Figure 1E) that contained PGP 9.5 labeled cells (Figure 1E) and nerve fibers (Figure 1F). No PGP 9.5 stained nerve fiber bundles were found and the amount of blood vessels were decreased compared with the 4 mm defects.

Quantification was conducted by scoring for the amount of PGP 9.5 positive nerve fibers that resulted in a rank order of 3 mm (score 2) <4 mm (score 3) >5 mm (score 1.33±0.21) with significant differences between 3 and 4 mm (p=0.002) and 4 and 5 mm defects (p=0.002) as shown in Figure 2A. Scoring of the amount of blood vessels demonstrated a rank order of 3 mm (score 1) <4 mm (score 2.5±0.22) >5 mm defects (score 1.17±0.22) with significant differences for the comparison of 3 and 4 mm (p=0.002) and 4 and 5 mm defects (p=0.004; Figure 2B).

To further distinguish nerve fibres and PGP 9.5 positive cells according to their cholinergic or adrenergic character, immunostainings with antibodies against VAChT and TH were performed, respectively. VAChT immunolabeling was found in the 3 mm defect in mast cells that were either localized in granulation tissue often near blood vessels or in the bone marrow frequently in the area surrounding the defect (Figure 3A). In addition VAChT immunolabeling was detected in nerve fibers (Figure 3B) and in nerve fiber bundles (Figure 3C) in the granulation tissue filling the bone defect. In sections of the 4 mm defect no VAChT labeled nerves were found but only immunopositive mast cells (Figure 3D). In the 5 mm defect only few VAChT immunopositive mast cells were detected in the granulation tissue (Figure 3E) while much more of them could be found in the bone marrow near the trabeculae (Figure 3F). In addition VAChT immunolabeled nerve fibers were present near blood vessels in the granulation tissue filling the bone defect (Figure 3G). Scoring of

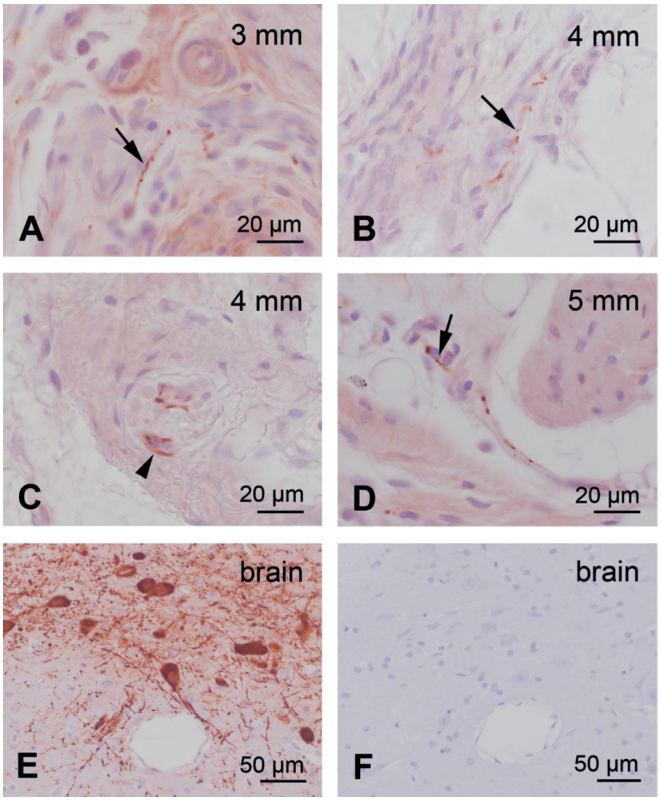

Figure 4. TH, defect healing. TH immunolabeling was determined in the 3 (A), 4 (B-C), and 5 mm defects (D). In the granulation tissue TH was found in nerve fibers (arrow, A-B, D) and in nerve fiber bundles (arrowhead, C). Brain was used as positive control (E). Primary antibody was omitted in the negative control (F).

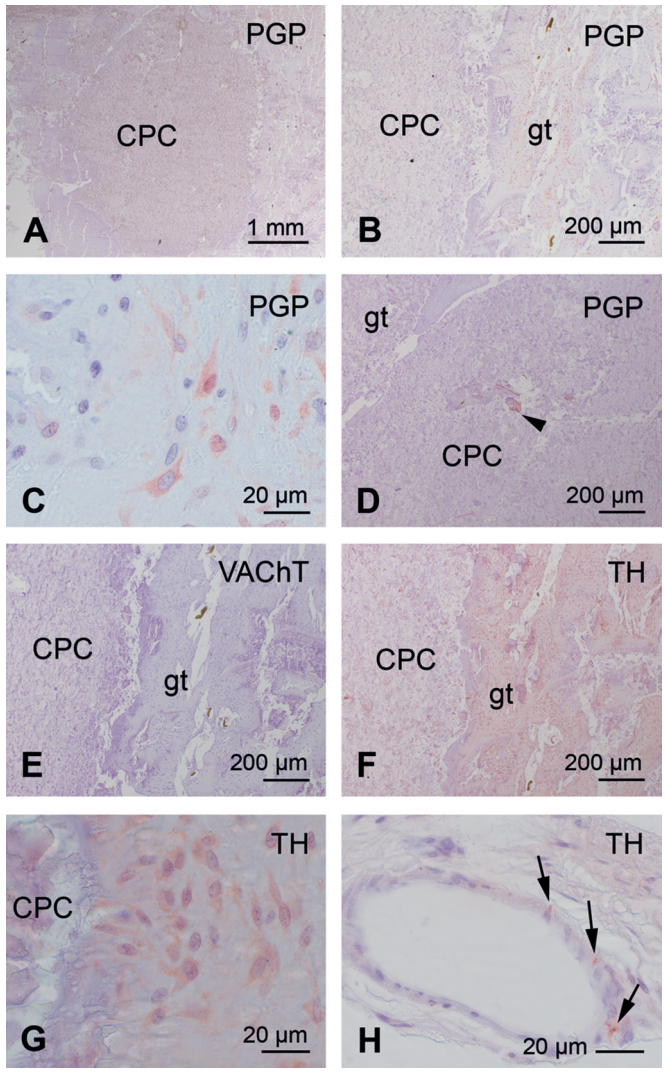

Figure 5. CPC. PGP (A-D) and TH (F-H) immunopositive cells were found in granulation tissue (gt) at the interface of CPC implants. PGP was also detected in the implant (arrow head, D) and TH in nerve fibers in the vessel wall (arrow, H). No VAChT signal was detected (E).

VAChT immunopositive nerve fibers resulted in statistically significant differences for the comparison of 3 mm (score 1.67±0.21) and 4 mm defects (score 0; p=0.002) as well as for the 4 and 5 mm defects (score 1; p=0.002, Figure 2C).

TH immunopositive nerve fibers were found in the granulation tissue that filled the 3, 4, and 5 mm defects (Figure 4). Mostly they were situated near blood vessels. Nerve fiber bundles containing single TH immunopositive nerves were determined in 4 mm defects. Scoring of TH immunopositive nerve fibers resulted in a rank order of 3 mm (score 2.17±0.17) >4 mm (1±0.32) <5 mm (score 1.67±0.21) defects. Significant differences were only determined for comparison of the amount of nerve nerve fibers between 3 and 4 mm defects (p=0.017, Figure 2D).

Sections of the brain were used as positive control for PGP 9.5, VAChT and TH antibodies (Figure 3H, Figure 4E) and specificity of staining was confirmed by performing of negative controls without the primary antibody (Figure 4F).

Nerve fibers at the implant interface of osteoporotic rat bone

In a second group of animals the defect was filled with several bone substitution materials. We analyzed whether neurons

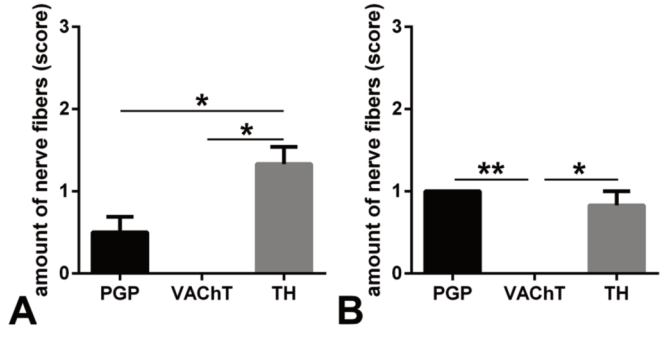

Figure 6. The amount of VAChT immunopositive nerve fibers were decreased at the interface of CPC (A) and CPC-Sr (B) implants. *p<0.05, **p<0.01; score 0=absent, 1=few, 2=moderate and, 3=high amount.

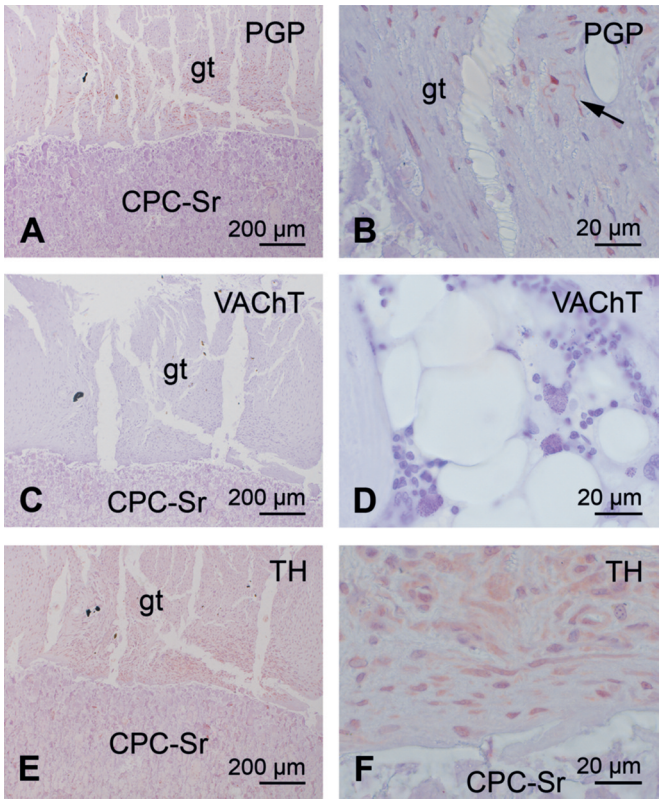

Figure 7. CPC-Sr. PGP (A-B) and TH (E-F) immunolabeling was found in cells and nerve fibers (arrow) in the granulation tissue (gt) at the interface of the CPC-Sr implant. VAChT immunolabeling was neither determined in the granulation tissue (C) nor in the mast cells in bone marrow (arrowhead, D).

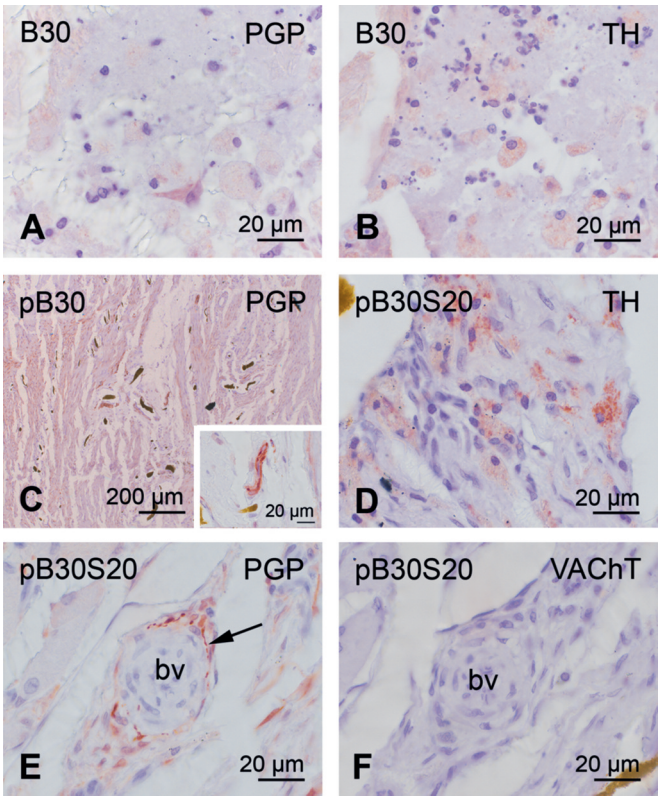

Figure 8. Composites of silica, collagen and strontium (B30, pB30, pB30S20). PGP (A) and TH (B) were found in cells at the interface of the B30 implant (70 wt% silica and 30 wt% collagen). After implantation of a porous formulation of B30 (pB30) PGP was detected in cells, nerve fibers, and nerve fiber bundles (C) while no TH labeling was observed. Modification of pB30 with strontium (pB30S20) leads to TH immunostaining in cells in the granulation tissue (D). PGP labeling was found in nerve fibers (arrow) near blood vessels (bv, E). No VAChT labeling occurred (F). Inset: higher magnification of C.

or cells expressing PGP 9.5, VAChT and TH were present at the implant interface. In the controls sections with 4 mm empty defects a high amount of PGP 9.5 immunopositive nerve fibers were detected (Figure 1C-D) whereas no VAChT immunopositive nerve fibers were found but several VAChT immunopositive mast cells (Figure 3D). Also some TH immunopositive nerve fibers could be detected in the granulation tissue filling the 4 mm empty defects (Figure 4C).

After implantation of CPC, PGP 9.5 immunopositive cells were found in the granulation tissue that is localized at the implant interface (Figure 5A-C) and even in the implant some PGP 9.5 immunopositive structures were observed (Figure 5D). No VAChT immunopositive structures were detected at the interface (Figure 5E). TH immunostaining was observed in the cytoplasm of cells and in a limited number of nerve fibers at the interface, the latter being localized in the blood vessel wall at the interface (Figure 5H). Scoring resulted in a rank order concerning labeled nerve fibers of TH (score 1.33±0.21) >PGP 9.5 (score 0.5±0.19) >VAChT (score 0) with significant differences between the amount of PGP 9.5 and TH (p=0.043) and TH and VAChT (p=0.01) labeled nerve fibers (Figure 6A).

The interface of the strontium modified CPC (CPC-Sr) revealed more PGP 9.5 immunopositive cells in the granulation tissue surrounding the implant (Figure 7A-B). Moreover some PGP 9.5 immunopositive nerve fibers were also detected (Figure 7B). Again no VAChT labeling was observed (score 0; Figure 7C-D). TH immunostaining was found in cells at the interface and also in some nerve fibers (Figure 7E-F). In contrast to empty defects no immunopositive nerve fiber bundles were found. Scoring of the immunopositive nerve fibers at the implant interface determined a significant decrease of VAChT immunopositive fibers (score 0) compared to PGP 9.5. (score 1, p=0.006) and TH (score 0.83±0.17, p=0.038; Figure 6B).

Defects filled with the xerogel B30 (Figure 8A-B) displayed two different PGP 9.5 immunopositive cell types at the interface: One cell type being big cells with foamy cytoplasm as usually found by macrophages. The other cell type was thinner and held processes. The macrophage-like cells were also immunopositive for TH (Figure 8B). No VAChT immunostaining

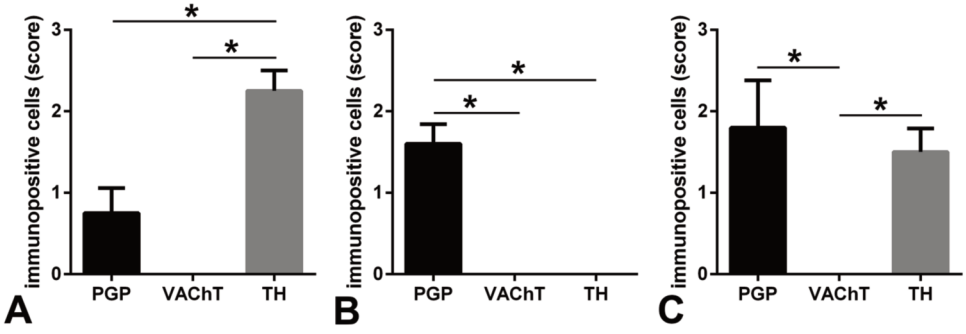

Figure 9. The amount of VAChT immunopositive cells were decreased at the interface of B30 implants (A) as well as in the granulation tissue replacing pB30 (B) and pB30S20 implants (C) implants. *p<0.05; score 0=absent, 1=few, 2=moderate, and 3=high amount.

was found at the interface of the xerogel B30 implant. The xerogel B30 was also implanted as particles embedded in a porous collagen scaffold (pB30). Six weeks of post operation follow-up time the implant was nearly fully resorbed whereby it was not possible to investigate the interface. Hence we analyzed the granulation tissue filling the bone defect where a high amount of PGP 9.5 immunopositive cells and fibers were found (Figure 8C). No VAChT and TH immunopositive structures could be identified. B30 particles were further implanted as the porous formulation with addition of strontium (pB30S20). Also this bone substitution material was nearly fully resorbed at the 6 week post-operation follow-up time point. In the defect-filling granulation tissue several PGP 9.5 (Figure 8E) as well as TH immunopositive neuronal processes and cells (Figure 8D) were found whereas no VAChT immunostaining could be detected (Figure 8F). For quantification of the xerogel implants the score included labeled nerve fibers as well as immunopositive cells. Scoring resulted in a significant increase of TH immunopositive structures at the interface of B30 (score 2.25±0.25) compared to PGP 9.5 (score 0.75±0.31, p=0.028) and VAChT (score 0, p=0.029; Figure 9A). PGP 9.5 immunopositive structures (score 1.6 ± 0.24) were increased in the granulation tissue replacing the pB30 implant compared to VAChT (score 0, p=0.016) and TH (score 0, p=0.016; Figure 9B). VAChT immunolabeled structures (score 0) were significant decreased compared to PGP 9.5 (score 1.8±0.58, p=0.03) and TH (score 1.5±0.29, p=0.01) in the granulation tissue replacing pB30S20 (Figure 9C).

Besides formulations of cement and xerogel also a metallic implant made of iron was inserted that was occupied with interconnected pores (Figure 10). The implant was developed for the reason of holding a degradable solid metal and giving the granulation tissue the chance to grow into the pores to improve bony stiffness. PGP 9.5 immunopositive nerve fibers and cells were found at the interface and in the pores of Fe, Fe-Sr, and Fe-BP implant (Figure 10A-E). Cells and nerve fibers positively stained for TH were detected at the interface of the Fe-Sr (Figure 10F) implant and to a lower content at the Fe-BP whereas at the Fe implant no TH labeling was present.

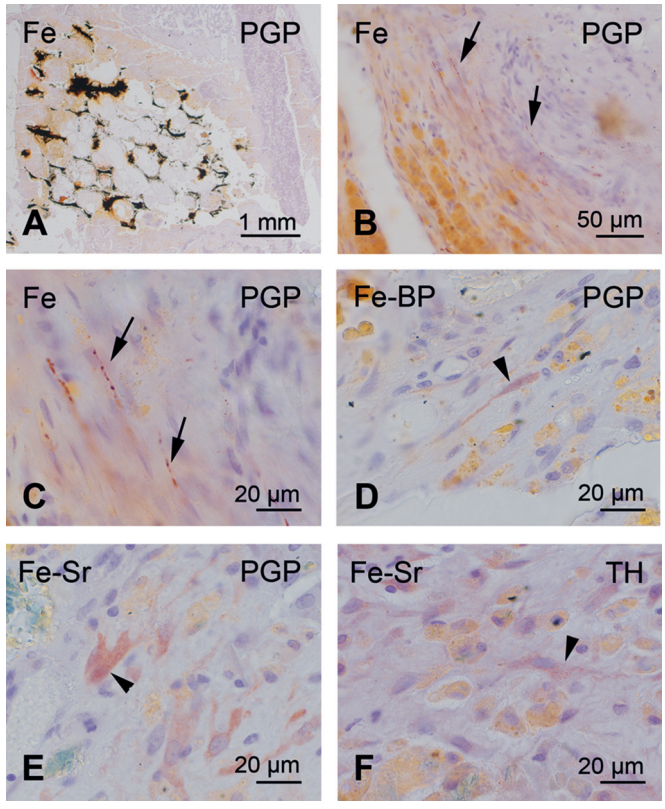

Figure 10. Porous iron implants (Fe) with coating of bisphosphonates (Fe-BP) or strontium (Fe-Sr). PGP immunopositive nerve fibers (arrow, B-C) and cells (arrowhead) were present at the interface and in the pores of Fe (A-C), Fe-BP (D), and Fe-Sr (E). TH was mainly detected in cells (arrowhead) at the interface of Fe-Sr (F).

No VAChT immunopositive labeling was determined at the interface and pores of the Fe, Fe-Sr, and Fe-BP implant. Scoring revealed significant more PGP 9.5 labeled structures (score 1.43±0.2) at the Fe implant than TH (score 0, p=0.006) and

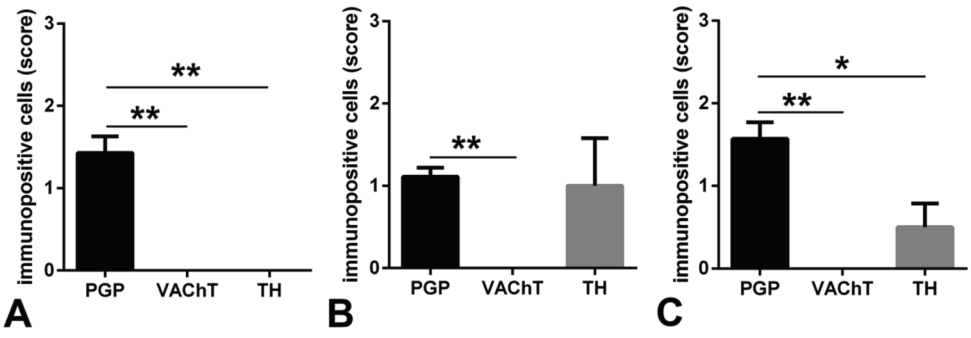

Figure 11. The amount of VAChT immunopositive cells were decreased after implantation of a porous Fe (A), Fe-Sr (B), and Fe-BP (C) implant. *p<0.05, **p<0.01; score 0=absent, 1=few, 2=moderate, and 3=high amount.

VAChT (score 0, p=0.006; Figure 11A). At the Fe-Sr implant, PGP 9.5 stained cells and fibers (score 1.11±0.11) were significant increased compared to VAChT (score 0, p=0.003) labeled structures whereas TH (score 1±0.58) showed no significant differences (Figure 11B). Scoring resulted in an increasing rank order of immunopositive structures at the Fe-BP implant of VAChT (score 0) <TH (score 0.5±0.29) <PGP 9.5 (score 1.57±0). The amount of PGP positive structures were significant increased compared to VAChT (p=0.006) and TH (p=0.042) immunopositive cells (Figure 11C).

Besides, the amount of PGP 9.5 immunopositive cells and nerve fibers found at the different bone substitution materials were compared. Comparison did not reveal significant differences between CPC (score 0.5±0.19) and CPC-Sr (score 1), B30 (score 0.75±0.31), pB30 (score 1.6±0.24) and pB30S20 (score 1.8±0.58) as well as Fe (score 1.42±0.2), Fe-BP (score 1.11±0.11) and Fe-Sr (score 1.57±0.2; Figure 12). The same statistical analysis was performed for TH immunolabeled cells and nerve fibers at the implant interface. Significant differences were detected between pB30 (score 0) and B30 (score 2.25±0.25, p=0.029) and between pB30 (score 0) and pB30S20 (score 1.5±0.29, p=0.029). No significant changes were determined for the comparison of CPC (score 1.33±0.21) and CPC-Sr (score 0.86±0.14) as well as for Fe (score 0), Fe-BP (score 1±0.58) and Fe-Sr (score 0.5±0.29; Figure 12).

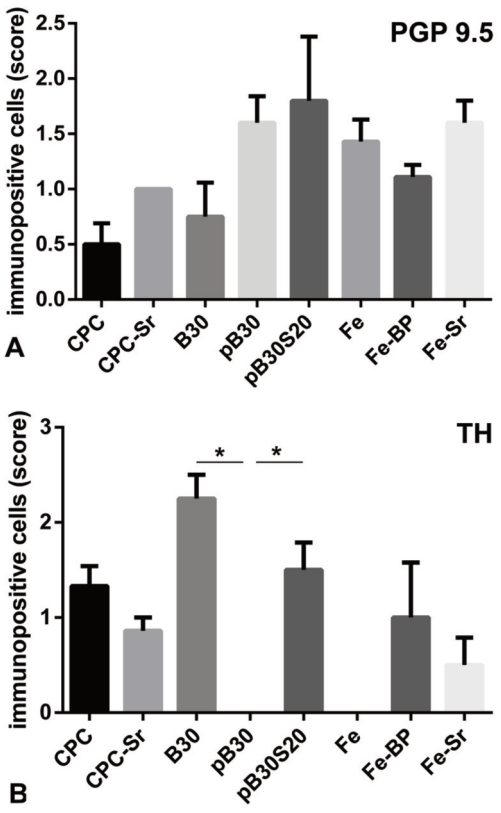

Figure 12. Comparison of PGP 9.5 (A) and TH (B) immunopositive cells and nerve fibers at the interface of the different implants. CPC= calcium phosphate bone cement. CPC-Sr= strontium modified CPC, B30= composite of silica and collagen, pB30= granula of B30, pB30S20= strontium modified granula of B30, Fe= porous iron implant, Fe-BP= Fe implant with coating of bisphosphonates, Fe-Sr= Fe implant with coating of strontium. *p<0.05.

Comparison of nerve fibers in sham and osteoporotic animals with bone defect and implant

In a third set of animals the nerve fiber density and quality were investigated in bone healthy (sham operated) and osteoporotic rats that received first a wedge-shaped osteotomy in the metaphysis of the distal part of the left femur. Afterwards the B30 implant was inserted. Immunohistochemistry for the nerve markers PGP 9.5, TH and VAChT was performed. In sham rats a high amount of PGP 9.5 immunopositive nerve fibers was found in the granulation tissue that surrounds the implant (score 3; Figure 13A,C). In the osteoporotic bone less PGP 9.5 positive fibers were detected (score 2; Figure 13B,D). Scoring of the fiber density resulted in a significant difference (p = 0.029) for the comparison of healthy and osteoporotic samples (Figure 14A). In both groups no TH immunopositive nerve fibers were observed at the implant interface (score 0,

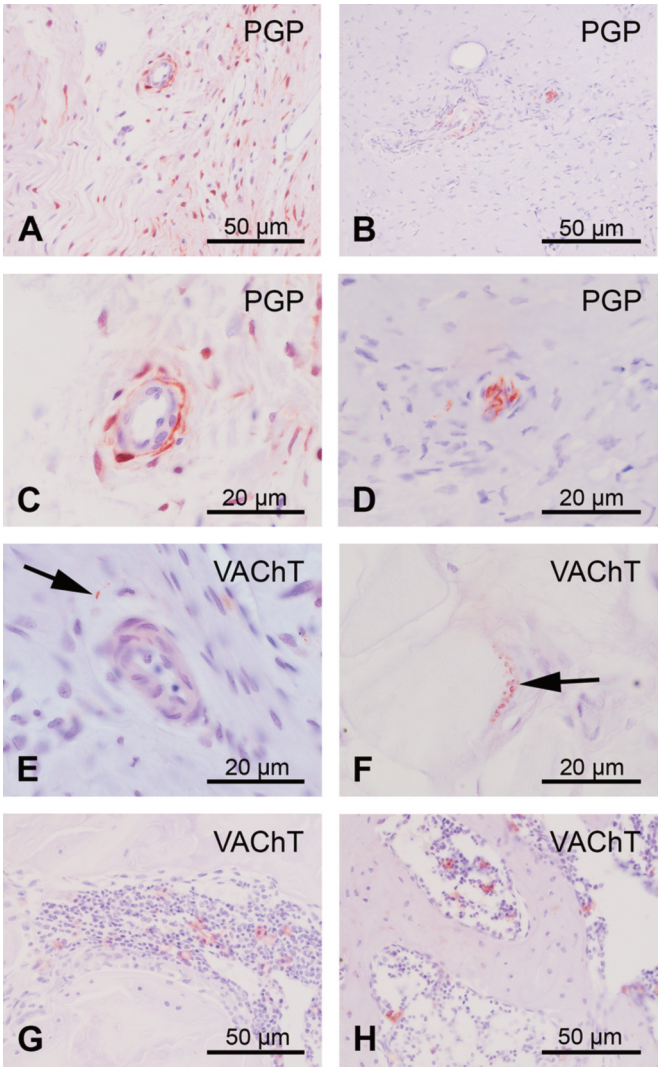

Figure 13. Comparison of nerve fibers in sham operated and osteoporotic bone defects with a composite implant of 70 wt% silica and 30 wt% collagen (B30). PGP 9.5 immunopositive nerve fibers were localized in the granulation tissue surrounding the implant of sham operated rats (A, C). Less PGP 9.5 stained nerve fibers were found in osteoporotic animals (B, D). VAChT immunopositive nerve fibers (arrow) were only detected in sham operated rats (E). Nerve fibers (arrow) at the muscles were used a positive control for the VAChT immunolabeling in osteopotoric rats (F). Only few VAChT positive mast cells were determined in sham animals (G) whereas the number and staining intensity increased in osteoporotic rats (H).

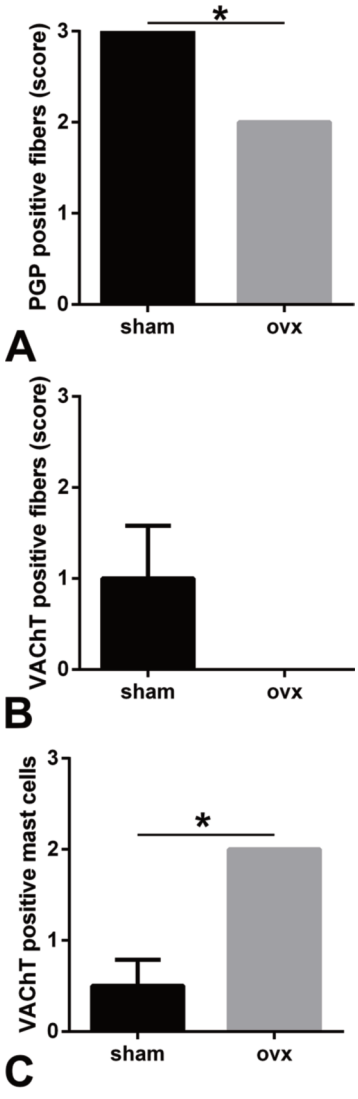

Figure 14. Defects of sham operated animals contained more PGP 9.5 (A) as well as more VAChT immunopositve nerve fibers (B) than animals after ovariectomy (ovx) whereas the amount of VAChT positive mast cells was increased in ovx compared to sham animals (C). *p<0.05, score 0=absent, 1=few, 2=moderate, and 3=high amount.

results not shown). Control tissue (brain sections) showed a distinct TH immunoreactivity. VAChT immunopositive nerve fibers were only found in the granulation tissue of healthy bone (score 1±0.58; Figure 13E) but not in the osteoporotic bone (score 0, Figure 14B). However the amount of VAChT positive nerve fibers was reduced compared to PGP 9.5 immunopositive neurons. Interestingly only a few VAChT immunopositive mast cells were determined in the healthy bone (score 0.5±0.29; Figure 13G) whereas a high amount of VAChT positive mast cells was found in the bone marrow of the osteoporotic rats (score 2, significant scoring value of p=0.029; Figure 13H and 14C). Also the staining intensity of VAChT was increased in mast cells of osteoporotic rats in comparison to sham operated animals.

Discussion

This study was conducted to receive details about the cholinergic innervation of bone defects with and without insertion of bone substitution materials in an animal model of

osteoporosis. Bone is innervated by sensory and autonomic nerves[9]. The autonomic nervous system consists of a sympathetic and parasympathetic route. The main neurotransmitter of the parasympathetic nervous system is acetylcholine (ACh) that is synthesized in the cytoplasm of neurons by the enzyme choline acetyltransferase (ChAT) out of choline and acetylcoenzym A[48]. In neurons VAChT transports cytoplasmic ACh into vesicles where it is accumulated and stored until it is released at the presynaptic button[49]. Thus, VAChT is used as a marker for nerve fibers that contain ACh[6]. Besides ACh these fibers can also synthesize and release vasoactive intestinal peptide (VIP). In several studies immunostaining with antibodies against VIP was used instead of VAChT[3,4,10,11,50]. VIP has been discussed as important regulator for osteoclastogenesis because it controls the secretion of osteoclastogenic factors by osteoblasts[51]. VIP immunopositive nerve fibers were localized in bone, periosteum, epiphysis, and occasionally near blood vessels[3,10]. Since the occurrence of VAChT and VIP immunopositive nerve fibers is different and influenced by estradiol[52] we decided to focus on cholinergic ACh containing nerve fibers identified by VAChT immunohistochemistry. Using mice with a neuron-specific knockout for the muscarinic acetylcholine receptor M3 (M3 mAChR) Shi et al. showed that the sympathetic activity in bone leads to a loss of bone mass, reduced bone formation by osteoblasts and increased bone resorption through up-regulation of osteoclasts[7]. ACh acts via stimulation of two classes of receptors: a) 5 different subtypes of G-protein coupled muscarinic receptors (mAChR) and b) homo- and heteropentameric nicotinic acetylcholine receptors (nAChR). The nAChR are ligand gated cation receptors that consists of 5 subunits. Nine different α-subunits and 4 different β-subunits are known to be present in mammals. The nAChR α2 subunit is always associated with a β-subunit in a heteropentameric nAChR. Interestingly, gene-deficient mice for the nAChR subunit α2 showed an increased bone resorption and a low bone mass[6] similar to the M3 mAChR knockout mice. Summarizing these both studies the cholinergic innervation seems to be involved in bone remodeling via stimulation of M3 mAChR and heteropentameric nAChR containing the α2-subunit. In addition to the neuronal cholinergic system a non-neuronal cholinergic system has been described[53]. All necessary molecular components of the cholinergic system e.g. enzymes for ACh synthesis, degradation, transporters, and receptors as well as ACh itself were also found in several non-neuronal cells. Some of the cholinergic molecules have already been confirmed to be present in bone, osteoblasts, mesenchymal stem cells and osteoclasts[6-8,54-56]. Thus the non-neuronal cholinergic system might also be involved in the regulation of bone remodeling. Because of the reduction as well as the absence of VAChT immunopositive nerve fibers as shown in the present study we suppose that the non-neuronal cholinergic system might hold the preferential function in bone in comparison to the neuronal cholinergic system. However, the role of the non-neuronal cholinergic system in osteoporotic bone defects with and without insertion of bone substitution materials has to be investigated thoroughly in a follow-up study. The aim of the present study was to analysis the presence of the cholinergic nerve fibers. VAChT immunopositive nerve fibers were found in the animal groups that received only the osteoporosis induction and the bone defect without additional implantation. Hence, this is the first study – up to our knowledge – that detected VAChT immunopositive nerve fibers in an osteoporosis animal model.

For experimental induction of osteoporosis an animal model was used where both ovaries were removed[26,27] and with them all the oocytes and surrounding follicle cells that produce estradiol. The female sex hormone estradiol protects the bone from enhanced bone rarefication. After menopause the follicle cells stopped their production of estradiol. Hence the estrogen concentration of the body is down-regulated. By numerous women this is subsequently followed by a loss of bone. The bone loss is intensified by additional malnutrition with un-balanced food that does not contain enough calcium and vitamin C/D[57]. To adjust our animal model used in the present study to the human situation of osteoporotic bone loss we conducted a bilateral ovariectomy and fed the animals (named ovx rats in our study) with a deficient diet were also calcium and vitamin C/D was reduced. Often big animals (sheep, goat, pig) are used as osteoporosis models because they mimic better the human situation than small animals[58]. However, since the keeping and breading of small animals is easier, cheaper, and faster we decided to use a small animal model for the first approach on cholinergic innervation in osteoporotic bone.

Re-innervation after fractures seems to be important for bone healing as suggested by several clinical as well as experimental studies[59,60]. Excessive callus formation with poor density and biomechanical stability is reported from patients with neurological defects as well as from rat fracture models[59,60]. New build nerves repopulate the defect before vascularization starts[18]. This is in line with findings from embryogenesis, where the appearance of nerve fibers and bone mineralization was correlated[11,61]. Neuropeptides e.g. substance P and calcitonin-gene-related peptide were supposed to be involved in bone healing[62] as well as in nociception[63]. Up to our knowledge, it was still ambiguous if cholinergic nerve fibers sprout into bone defects. Thus, we analyzed in the first animal model of the present study the cholinergic re-innervation in bone defects of different sizes. We determined no VAChT immunopositive nerves in defects of 4 mm whereas they were present in 3 and 5 mm defects. Generally, the highest number of nerve fibers was observed in 4 mm defects as identified by PGP 9.5 immunohistochemistry. The increase of PGP 9.5 positive nerve fibers was correlated with the re-vascularization of bone defects. However the PGP 9.5 positive nerves were not cholinergic. Since the amount of TH immunopositive fibers was also declined we suspect that the PGP 9.5. nerve fibers in the 4 mm defects were neither cholinergic nor adrenergic. Thus, they might belong to the sensitive nervous system which should be proven in a follow-up study.

Since neuronal disorders lead to a decreased bone growth, turnover and repair[15-19] the hypothesis arose that in return in bone pathogenesis the innervation could be declined. And in-

deed a dramatic decrease of innervation density was reported in bone after ovariectomy[23]. This decrease in nerve fibers has been confirmed in our third animal study. In addition we analyzed the quality of the nerve fibers in our third animal study where we compared non-osteoporotic rats with bony defects and insertion of substitution material with osteoporotic animals that received the same bone defect and implant. Thereby we found that the amount of PGP 9.5 and VAChT immunopositive nerve fibers were declined in osteoporosis. Thus, we presume that osteoporosis caused a decrease in cholinergic nerve fibers. In our second animal study we investigated whether the decline in cholinergic nerve fibers is influenced by the choice of bone substitution material. Eight different bone substitution materials were tested. Cholinergic nerve fibers were found in none of them. Thus, we guess, that the down-regulation of nerve fibers due to insertion of bone substitution materials mostly affects cholinergic neurons.

In healthy bone VAChT immunopositive nerve fibers were found in the medullary intertrabecular spaces one to three cell layers away from the trabecular surface in the distal metaphyseal area of femur[6]. In our animal studies VAChT immunopositive nerve fibers were only localized in the granulation tissue filling the bone defect and to a lower degree surrounding blood vessels of the periosteum. In addition to the labelling of nerve fibers, VAChT immunoreaction was found in mast cells in the granulation tissue as well as in the bone marrow. Interestingly, the amount of VAChT positive mast cells in the bone marrow increased after induction of osteoporosis. Mast cells are resident cells of the innate immune system that play a key role in inflammation as early effectors. Recently mast cells were identified as target of the cholinergic anti-inflammatory pathway since they were inhibited by the blockers of α7-nAChR[64]. Moreover ACh and nicotine are involved in the degranulation of mast cells and subsequently in histamine secretion[65,66]. Dermal mast cells and the human mast cell line HMC-1 express several nAChR, mAChR, and the ACh degrading enzyme acetylcholine esterase (AChE)[66]. It has been reported that mast cells also express the transporter SLC10A4 that belongs to the sodium-bile acid cotransporter family and is announced to be a transporter for acetylcholine in cholinergic neurons as well as in several non-neuronal cells[67,68]. Contrarily, ACh synthesizing enzymes were not present in dermal mast cells and a human mast cell line[66].

In the first set of animals where we compared the different bone defect sizes (3, 4, and 5 mm), most VAChT immunopositive fibers were found in 5 mm defects. Rats with 5 mm defects showed a delayed healing. After 6 week postoperative follow-up time the defect was filled with newly generated granulation tissue. In general, fracture healing is subdivided into a first period of inflammation, a second of callus formation and a last period of repair[69]. The defect healing of the 5 mm defect seems to go beyond the inflammatory period of the healing process. Thus, it can be speculated that ACh is involved in the termination of the inflammatory period. Even if this hypothesis is only speculative and needs of course an approval in a bone defect model where different time points will be analyzed, the assumption should be reflected on the basis of the cholinergic anti-inflammatory pathway[70]. This pathway describes that neuronal released ACh binds to the α7-nAChR on the surface of macrophages and down-regulates the secretion of pro-inflammatory cytokines like tumor-necrosis-factor-α (TNFα)[70]. Hence this signaling pathway leads to a reduction of inflammation. However, only a few VAChT immunopositive nerve fibers were detected in the granulation tissue filling the 3 and 4 mm defects. The 3 mm defects showed nearly complete osseous consolidation[28]. The 4 mm defects are typical critical size defects without bony bridging between the fragments but filled with granulation tissue and started to build up callus 6 weeks after osteotomy. Besides nerve fibers VAChT was also found in some of the mast cells in bone marrow between the trabeculae and surrounding blood vessels in the granulation tissue filling the defect. In our rat osteoporosis bone defect model VAChT immunolabeling was detected only in one part of the mast cells. Not all bone marrow and tissue mast cells were positive. Most VAChT immunopositive mast cells were found in animals that received a 5 mm defect and in the osteoporotic animals with bone defect and insertion of the B30 bone substitution material in the third set of animals where we compared non-osteoporotic and osteoporotic rats.

To our knowledge this is the first study that investigates whether insertion of different bone substitution materials into bony defects influenced the presence of cholinergic nerve fibers at the interface of bone substitution materials. We analyzed whether cholinergic nerve fibers were present at the interface of different implants in osteoporotic animals. Unexpectedly, we did not find any VAChT immunopositive nerves. Thus, immunohistochemical staining for antibodies against the pan-neuronal marker PGP 9.5 and the sympathetic marker TH were conducted. TH is the rate-limiting enzyme in the biosynthesis pathway of catecholamines. We observed an estimated but not significant increase in the amount of TH immunopositive cells and fibers at the interface of CPC implants compared to CPC-Sr (Figure 12B). In addition more TH immunolabelled structures appeared around B30 implants compared to pB30 and pB30S20 as well as at the interface of Fe-BP compared to Fe-Sr and plain Fe (Figure 12B). Modification of CPC with strontium lead to enhanced bone formation in defects of osteoporotic bone[29]. Accordingly the higher amount of TH positive structures was detected in the surrounding of the bone substitution material that was less effective in bone formation compared to CPC-Sr. This assumption is confirmed by reports that revealed a decline in bone formation, an inhibition of osteoblast proliferation, and enhanced osteoclastogenesis as consequence of adrenergic signaling (reviewed in[71]). Hence, the sympathetic part of the autonomic nervous system seemed to be involved in bone loss whereas the cholinergic part enhanced bone mass accrual as shown by usage of cholinergic knockout-mice[6,7].

PGP 9.5 is used as common marker for nerves of all qualities since it is specific for a 27 kDa ubiquitin-protein hydrolase that is localized in the cytoplasm of neurons and cells of the diffuse neuroendocrine system and related tumors. A high

amount of PGP 9.5 immunopositive cells, nerve fibers, and even nerve fiber bundles were found in the granulation tissue filling the bone defect. At the interface of implanted bone substitution materials also PGP 9.5 immunopositive structures were found. Their amount differed between the groups. Only in animals without implant or with the already resorbed porous xerogels (pB30, pB30S20) PGP 9.5 immunopositive nerve fiber bundles were determined. An estimated but not significant increase in the amount of PGP 9.5 immunopositive structures was detected in the animal group of CPC-Sr compared to CPC, pB30S20 compared to B30 and pB30, as well as in Fe-Sr compared to Fe and Fe-BP. On the background of the review of Garcia-Castellano et al.[21] where the authors hypothesize that a lack of neuronal control might lead to a delayed fracture healing we assume that implants with a high number of nerve fibers in the circumference are most suitable for defect healing in osteoporotic bone. However as a consequence of the studies on the bone architecture of cholinergic receptor knockout mice that reported a loss in bone mass[6-8] we would like to specify the hypothesis on innervation. We hypothesize that an increase in cholinergic nerve fibers surrounding an implant will identify the most suitable bone substitution material at least for the osteoporotic bone. This presumption is of course speculative and has to be proven very carefully since the used bone substitution materials was thoroughly tested *in vitro* before application in the animal model and all seemed to be very suitable for usage in osteoporotic bone. However, there is still a big difference between *in vitro* and *in vivo* studies. The obvious down-regulation of innervation in defects with additional insertion of bone substitution material might give rise to establish materials that are also compliant to nerve fibers in addition to their compatibility to mesenchymal stem cells, osteoblasts, and osteoclast.

However, a relative up-regulation of PGP 9.5 immunoreactivity was found in animals with bone substitution materials that were functionalized with strontium. Experimental analysis with strontium showed that it enhances osteoblasts forming new bone and slows down the bone degradation by osteoclasts especially in osteoporotic bone[29,35]. Further, administration of strontium ranelate to osteoporotic patients also showed beneficial effects[35]. Thus one of the future paths to establish suitable bone substitution material for osteoporotic patients might be the modification with elements that improve bone mass and structure. As a consequence of the present study the innervation might be used as an additional factor for the evaluation of bone substitution materials. The cholinergic system seems to come to the fore in bone health. Recently Eimar et al. (2013) reported in a review that there is a tight relationship between low bone mineral density and failure in cholinergic reception in peripheral organs e.g. respirator system, gastrointestinal system, salivary glands, and pancreas[9]. In pancreas there is a decrease in cholinergic activity due to a damage of the muscarinic acetylcholine receptor subtype M3 that results in diabetes type 1 and 2 and in bone loss[72-74]. Thus the cholinergic activity of several organ systems and the metabolism are linked to bone remodeling and should be taken in account for clinical interventions as well as for the establishment of new bone substitution materials.

In conclusion we could show that cholinergic nerve fibers occur in osteoporotic bone but not at the interface of bone substitution materials. Even a decrease in sympathetic fibers and neurons stained by the pan-neuronal marker PGP 9.5 were demonstrated. Thus, one of the future prospects for improvement of implants should be the increase of compatibility to nerve fibers.

Acknowledgements

The authors thank Rainer Braun, Martina Fink, Ida Oberst, and Tanja Rehling for skillful technical assistance, and Dr. Janet Beckmann for language approval. This study was supported by DFG (SFB/TRR 79 projects B7, T1, T2, M2, and M3).

References

1. Tarantino U, Cerocchi I, Scialdoni A, Saturnino L, Feola M, Celi M, et al. Bone healing and osteoporosis. Aging Clin Exp Res 2011;23:62-4.
2. Nakahama K. Cellular communications in bone homeostasis and repair. Cell Mol Life Sci 2010;67:4001-9.
3. Hill EL, Elde R. Distribution of CGRP-, VIP-, D beta H, SP-, and NPY-immunoreactive nerves in the periosteum of the rat. Cell Tissue Res 1991;264:469-80.
4. Hohmann EL, Elde RP, Rysavy JA, Einzig S, Gebhard RL. Innervation of periosteum and bone by sympathetic vasoactive intestinal peptide-containing nerve fibers. Science 1986;232:868-71.
5. Serre CM, Farlay D, Delmas PD, Chenu C. Evidence for a dense and intimate innervation of the bone tissue, including glutamate-containing fibers. Bone 1999;25:623-9.
6. Bajayo A, Bar A, Denes A, Bachar M, Kram V, Attar-Namdar M, et al. Skeletal parasympathetic innervation communicates central IL-1 signals regulating bone mass accrual. Proc Natl Acad Sci U S A 2012;109:15455-60.
7. Shi Y, Oury F, Yadav VK, Wess J, Liu XS, Guo XE, et al. Signaling through the M(3) muscarinic receptor favors bone mass accrual by decreasing sympathetic activity. Cell Metab 2010;11:231-8.
8. Kliemann K, Kneffel M, Bergen I, Kampschulte M, Langheinrich AC, Durselen L, et al. Quantitative analyses of bone composition in acetylcholine receptor M3R and alpha7 knockout mice. Life Sci 2012;91:997-1002.
9. Eimar H, Tamimi I, Murshed M, Tamimi F. Cholinergic regulation of bone. J Musculoskelet Neuronal Interact 2013;13:124-32.
10. Bjurholm A, Kreicbergs A, Terenius L, Goldstein M, Schultzberg M. Neuropeptide Y-, tyrosine hydroxylase- and vasoactive intestinal polypeptide-immunoreactive nerves in bone and surrounding tissues. J Auton Nerv Syst 1988;25:119-25.
11. Sisask G, Bjurholm A, Ahmed M, Kreicbergs A. The development of autonomic innervation in bone and joints of the rat. J Auton Nerv Syst 1996;59:27-33.

12. Gajda M, Litwin JA, Tabarowski Z, Zagolski O, Cichocki T, Timmermans JP, et al. Development of rat tibia innervation: colocalization of autonomic nerve fiber markers with growth-associated protein 43. Cells Tissues Organs 2010;191:489-99.
13. Asmus SE, Parsons S, Landis SC. Developmental changes in the transmitter properties of sympathetic neurons that innervate the periosteum. J Neurosci 2000; 20:1495-504.
14. Tien D, Ohara PT, Larson AA, Jasmin L. Vagal afferents are necessary for the establishment but not the maintenance of kainic acid-induced hyperalgesia in mice. Pain 2003;102:39-49.
15. Cherruau M, Facchinetti P, Baroukh B, Saffar JL. Chemical sympathectomy impairs bone resorption in rats: a role for the sympathetic system on bone metabolism. Bone 1999;25:545-51.
16. Edoff K, Hellman J, Persliden J, Hildebrand C. The developmental skeletal growth in the rat foot is reduced after denervation. Anat Embryol (Berl) 1997;195:531-8.
17. Hukkanen M, Konttinen YT, Santavirta S, Nordsletten L, Madsen JE, Almaas R, et al. Effect of sciatic nerve section on neural ingrowth into the rat tibial fracture callus. Clin Orthop Relat Res 1995;(311):247-57.
18. Li J, Ahmad T, Spetea M, Ahmed M, Kreicbergs A. Bone reinnervation after fracture: a study in the rat. J Bone Miner Res 2001;16:1505-10.
19. Jones KB, Mollano AV, Morcuende JA, Cooper RR, Saltzman CL. Bone and brain: a review of neural, hormonal, and musculoskeletal connections. Iowa Orthop J 2004;24:123-32.
20. Freehafer AA, Mast WA. Lower Extremity Fractures in Patients with Spinal-Cord Injury. J Bone Joint Surg Am 1965;47:683-94.
21. Garcia-Castellano JM, Diaz-Herrera P, Morcuende JA. Is bone a target-tissue for the nervous system? New advances on the understanding of their interactions. Iowa Orthop J 2000;20:49-58.
22. Retief DH, Dreyer CJ. Effects of neural damage on the repair of bony defects in the rat. Arch Oral Biol 1967;12:1035-9.
23. Burt-Pichat B, Lafage-Proust MH, Duboeuf F, Laroche N, Itzstein C, Vico L, et al. Dramatic decrease of innervation density in bone after ovariectomy. Endocrinology 2005;146:503-10.
24. Nauth A, Miclau T 3rd, Bhandari M, Schemitsch EH. Use of osteobiologics in the management of osteoporotic fractures. J Orthop Trauma 2011;25 Suppl 2:S51-5.
25. Ma XL, Xing D, Ma JX, Xu WG, Wang J, Chen Y. Balloon kyphoplasty versus percutaneous vertebroplasty in treating osteoporotic vertebral compression fracture: grading the evidence through a systematic review and meta-analysis. Eur Spine J 2012;21:1844-59.
26. Govindarajan P, Schlewitz G, Schliefke N, Weisweiler D, Alt V, Thormann U, et al. Implications of combined ovariectomy/multi-deficiency diet on rat bone with age-related variation in bone parameters and bone loss at multiple skeletal sites by DEXA. Med Sci Monit Basic Res 2013;19:76-86.
27. Heiss C, Govindarajan P, Schlewitz G, Hemdan NY, Schliefke N, Alt V, et al. Induction of osteoporosis with its influence on osteoporotic determinants and their interrelationships in rats by DEXA. Med Sci Monit 2012; 18:BR199-207.
28. Alt V, Thormann U, Ray S, Zahner D, Durselen L, Lips K, et al. A new metaphyseal bone defect model in osteoporotic rats to study biomaterials for the enhancement of bone healing in osteoporotic fractures. Acta Biomater 2013;9:7035-42.
29. Thormann U, Ray S, Sommer U, Elkhassawna T, Rehling T, Hundgeburth M, et al. Bone formation induced by strontium modified calcium phosphate cement in critical-size metaphyseal fracture defects in ovariectomized rats. Biomaterials 2013;34:8589-98.
30. Alt V, Kogelmaier DV, Lips KS, Witt V, Pacholke S, Heiss C, et al. Assessment of angiogenesis in osseointegration of a silica-collagen biomaterial using 3D-nano-CT. Acta Biomater 2011;7:3773-9.
31. Schumacher M, Lode A, Helth A, Gelinsky M. A novel strontium(II)-modified calcium phosphate bone cement stimulates human-bone-marrow-derived mesenchymal stem cell proliferation and osteogenic differentiation *in vitro*. Acta Biomater 2013;9:9547-57.
32. Schumacher M, Henss A, Rohnke M, Gelinsky M. A novel and easy-to-prepare strontium(II) modified calcium phosphate bone cement with enhanced mechanical properties. Acta Biomater 2013;9:7536-44.
33. Bajammal SS, Zlowodzki M, Lelwica A, Tornetta P, 3rd, Einhorn TA, Buckley R, et al. The use of calcium phosphate bone cement in fracture treatment. A meta-analysis of randomized trials. J Bone Joint Surg Am 2008; 90:1186-96.
34. Khairoun I, Boltong MG, Driessens FC, Planell JA. Effect of calcium carbonate on the compliance of an apatitic calcium phosphate bone cement. Biomaterials 1997; 18:1535-9.
35. Marie PJ. Strontium ranelate in osteoporosis and beyond: identifying molecular targets in bone cell biology. Mol Interv 2010;10:305-12.
36. Heinemann S, Heinemann C, Bernhardt R, Reinstorf A, Nies B, Meyer M, et al. Bioactive silica-collagen composite xerogels modified by calcium phosphate phases with adjustable mechanical properties for bone replacement. Acta Biomater 2009;5:1979-90.
37. Heinemann S, Coradin T, Worch H, Wiesmann HP, Hanke T. Possibilities and limitations of preparing silica/collagen/hydroxyapatite composite xerogels as load-bearing biomaterials. Composites Science and Technology 2011; 71:1873-80.
38. Heinemann S, Heinemann C, Wenisch S, Alt V, Worch H, Hanke T. Calcium phosphate phases integrated in silica/collagen nanocomposite xerogels enhance the

bioactivity and ultimately manipulate the osteoblast/osteoclast ratio in a human co-culture model. Acta Biomater 2013;9:4878-88.
39. Han P, Wu C, Xiao Y. The effect of silicate ions on proliferation, osteogenic differentiation and cell signalling pathways (WNT and SHH) of bone marrow stromal cells. Biomaterials Science 2013;1:379-92.
40. Peuster M, Wohlsein P, Brugmann M, Ehlerding M, Seidler K, Fink C, et al. A novel approach to temporary stenting: degradable cardiovascular stents produced from corrodible metal-results 6-18 months after implantation into New Zealand white rabbits. Heart 2001;86:563-9.
41. Peuster M, Fink C, Wohlsein P, Bruegmann M, Gunther A, Kaese V, et al. Degradation of tungsten coils implanted into the subclavian artery of New Zealand white rabbits is not associated with local or systemic toxicity. Biomaterials 2003;24:393-9.
42. Peuster M, Kaese V, Wuensch G, Wuebbolt P, Niemeyer M, Boekenkamp R, et al. Dissolution of tungsten coils leads to device failure after transcatheter embolisation of pathologic vessels. Heart 2001;85:703-4.
43. Liu B, Zheng YF. Effects of alloying elements (Mn, Co, Al, W, Sn, B, C and S) on biodegradability and *in vitro* biocompatibility of pure iron. Acta Biomaterialia 2011; 7:1407-20.
44. Stephani G, Andersen O, Gohler H, Kostmann C, Kummel K, Quadbeck P, et al. Iron based cellular structures - Status and prospects. Advanced Engineering Materials 2006;8:847-52.
45. Wegener B, Sievers B, Utzschneider S, Muller P, Jansson V, Rossler S, et al. Microstructure, cytotoxicity and corrosion of powder-metallurgical iron alloys for biodegradable bone replacement materials. Materials Science and Engineering B-Advanced Functional Solid-State Materials 2011;176:1789-96.
46. Carulli C, Civinini R, Matassi F, Villano M, Innocenti M. The use of anti-osteoporosis drugs in total knee arthroplasty. Aging Clin Exp Res 2011;23:38-9.
47. Fernandez E, Ginebra MP, Boltong MG, Driessens FCM, Ginebra J, DeMaeyer EAP, et al. Kinetic study of the setting reaction of a calcium phosphate bone cement. Journal of Biomedical Materials Research 1996;32:367-74.
48. Jope RS, Jenden DJ. The utilization of choline and acetyl coenzyme A for the synthesis of acetylcholine. J Neurochem 1980;35:318-25.
49. Erickson JD, Varoqui H, Schafer MK, Modi W, Diebler MF, Weihe E, et al. Functional identification of a vesicular acetylcholine transporter and its expression from a "cholinergic" gene locus. J Biol Chem 1994;269:21929-32.
50. Togari A. Adrenergic regulation of bone metabolism: possible involvement of sympathetic innervation of osteoblastic and osteoclastic cells. Microsc Res Tech 2002;58:77-84.
51. Persson E, Lerner UH. The neuropeptide VIP regulates the expression of osteoclastogenic factors in osteoblasts. J Cell Biochem 2011;112:3732-41.
52. Kozlowska A, Majewski M, Jana B. Changes in the Cholinergic Innervation Pattern of Porcine Ovaries with Cysts Induced by Dexamethasone Administration. J Mol Neurosci 2014.
53. Wessler I, Kirkpatrick CJ. Acetylcholine beyond neurons: the non-neuronal cholinergic system in humans. Br J Pharmacol 2008;154:1558-71.
54. En-Nosse M, Hartmann S, Trinkaus K, Alt V, Stigler B, Heiss C, et al. Expression of non-neuronal cholinergic system in osteoblast-like cells and its involvement in osteogenesis. Cell Tissue Res 2009;338:203-15.
55. Sato T, Abe T, Chida D, Nakamoto N, Hori N, Kokabu S, et al. Functional role of acetylcholine and the expression of cholinergic receptors and components in osteoblasts. FEBS Lett 2010;584:817-24.
56. Liu PS, Chen YY, Feng CK, Lin YH, Yu TC. Muscarinic acetylcholine receptors present in human osteoblast and bone tissue. Eur J Pharmacol 2011;650:34-40.
57. Lips P, Bouillon R, van Schoor NM, Vanderschueren D, Verschueren S, Kuchuk N, et al. Reducing fracture risk with calcium and vitamin D. Clin Endocrinol (Oxf) 2010; 73:277-85.
58. Reinwald S, Burr D. Review of nonprimate, large animal models for osteoporosis research. J Bone Miner Res 2008; 23:1353-68.
59. Aro H. Effect of nerve injury on fracture healing. Callus formation studied in the rat. Acta Orthop Scand 1985; 56:233-7.
60. Perkins R, Skirving AP. Callus formation and the rate of healing of femoral fractures in patients with head injuries. J Bone Joint Surg Br 1987;69:521-4.
61. Sisask G, Bjurholm A, Ahmed M, Kreicbergs A. Ontogeny of sensory nerves in the developing skeleton. Anat Rec 1995;243:234-40.
62. Li J, Kreicbergs A, Bergstrom J, Stark A, Ahmed M. Site-specific CGRP innervation coincides with bone formation during fracture healing and modeling: A study in rat angulated tibia. J Orthop Res 2007;25:1204-12.
63. Saxler G, Loer F, Skumavc M, Pfortner J, Hanesch U. Localization of SP- and CGRP-immunopositive nerve fibers in the hip joint of patients with painful osteoarthritis and of patients with painless failed total hip arthroplasties. Eur J Pain 2007;11:67-74.
64. de Haan JJ, Hadfoune M, Lubbers T, Hodin CM, Lenaerts K, Ito A, et al. Lipid-rich enteral nutrition regulates mucosal mast cell activation via the vagal anti-inflammatory reflex. Am J Physiol Gastrointest Liver Physiol 2013; 305(5):G383-91.
65. Blandina P, Fantozzi R, Mannaioni PF, Masini E. Characteristics of histamine release evoked by acetylcholine in isolated rat mast cells. J Physiol 1980;301:281-93.
66. Radosa J, Dyck W, Goerdt S, Kurzen H. The cholinergic system in guttate psoriasis with special reference to mast cells. Exp Dermatol 2011;20:677-9.
67. Burger S, Doring B, Hardt M, Beuerlein K, Gerstberger R, Geyer J. Co-expression studies of the orphan carrier protein Slc10a4 and the vesicular carriers VAChT and

VMAT2 in the rat central and peripheral nervous system. Neuroscience 2011;193:109-21.
68. Borges K. Slc10A4 - what do we know about the function of this "secret ligand carrier" protein? Exp Neurol 2013;248:258-61.
69. Claes L, Recknagel S, Ignatius A. Fracture healing under healthy and inflammatory conditions. Nat Rev Rheumatol 2012;8:133-43.
70. Czura CJ, Tracey KJ. Autonomic neural regulation of immunity. J Intern Med 2005;257:156-66.
71. Elefteriou F, Campbell P, Ma Y. Control of bone remodeling by the peripheral sympathetic nervous system. Calcif Tissue Int 2014;94:140-51.
72. Tuominen JT, Impivaara O, Puukka P, Ronnemaa T. Bone mineral density in patients with type 1 and type 2 diabetes. Diabetes Care 1999;22:1196-200.
73. Gautam D, Han SJ, Duttaroy A, Mears D, Hamdan FF, Li JH, et al. Role of the M3 muscarinic acetylcholine receptor in beta-cell function and glucose homeostasis. Diabetes Obes Metab 2007;9 Suppl 2:158-69.
74. Arends J, Wagner ML, Willms BL. Cholinergic muscarinic receptor blockade suppresses arginine- and exercise-induced growth hormone secretion in type I diabetic subjects. J Clin Endocrinol Metab 1988;66:389-94.